https://doi.org/10.5194/essd-2026-158
Preprint. Discussion started: 31 March 2026

Tracking recent extremes and interannual variability of global fire emissions using a near-real-time extension to the Global Fire Emissions Database

[1]Yang Chen, [2]Guido R. van der Werf, [1]Mingquan Mu, [3]Dave van Wees, [4]Joanne V. Hall, [4]Louis Giglio, [2]Roland Vernooij, [5]Douglas C. Morton, [1]Li Xu, [6]Tianjia Liu, [1]Rebecca C. Scholten, [7]Shane R. Coffield, [5]Melanie B. Follette-Cook, [5]Lesley Ott, [1]James T. Randerson

[1]Department of Earth System Science, University of California, Irvine, 92612, USA
[2]Meteorology and Air Quality Group, Wageningen University & Research, Wageningen, the Netherlands
[3]BeZero Carbon, London, UK
[4]Department of Geographical Sciences, University of Maryland, College Park, MD, USA
[5]Biospheric Sciences Laboratory, NASA Goddard Space Flight Center, Greenbelt, MD, USA
[6]Department of Geography, University of British Columbia, Vancouver, BC, Canada
[7]Earth System Science Interdisciplinary Center, University of Maryland, College Park, MD, USA

Correspondence to: Yang Chen (yang.chen@uci.edu)

Abstract. The Global Fire Emissions Database (GFED) is widely used to quantify spatiotemporal variability and long-term trends in burned area and fire emissions, supporting assessments of fire impacts on ecosystems and atmospheric composition. GFED has historically relied on observations from the Moderate Resolution Imaging Spectroradiometer (MODIS), but orbital drift and planned sensor decommissioning pose challenges for maintaining record continuity and near-real-time (NRT) monitoring. Here we present the GFED5 near-real-time extension (GFED5NRT), a global fire emissions dataset that enables daily NRT analyses using active fire observations from the Visible Infrared Imaging Radiometer Suite (VIIRS). GFED5NRT uses biome- and region-specific lookup tables of effective fire area and fuel consumption, derived from VIIRS observations and standard GFED5 datasets, to estimate burned area and emissions from VIIRS active fire counts in a manner consistent with the GFED5 time series. Comparisons with GFED5 and independent datasets show strong agreement in spatial patterns, seasonal cycles, and interannual variability of fire activity. GFED5NRT captures recent major fire extremes and provides daily global NRT estimates of burned area and emissions for multiple trace gases and aerosols. Together, GFED5 and GFED5NRT provides a coherent framework for long-term analyses and NRT monitoring of evolving fire regimes in a changing climate. The GFED5NRT dataset is publicly available at https://doi.org/10.5281/zenodo.18702700 (Chen et al., 2026).

Short Summary. Fire patterns are changing, partly due to climate change. While the Global Fire Emissions Database (GFED) is a key tool for tracking fire impacts, its main satellite sensors are retiring. We introduce GFED5NRT, a new extension using modern VIIRS satellite data to provide daily, real-time updates on fires and smoke. By bridging past records with current observations, this system helps scientists and the public monitor extreme fire events and their effects on our changing planet.

1. Overview

Recent studies have documented substantial shifts in the frequency and intensity of global wildfires, driven primarily by climate change and land-use dynamics (Jones et al., 2022). Although total global burned area has declined over recent decades (approximately -1.2% yr^{-1}), largely due to reduced fire activity in African savannas (Andela et al., 2017) and croplands worldwide (Hall et al., 2024), fire risk has intensified in many other regions. Prolonged droughts and rising temperatures have increased the occurrence of extreme fire weather (Jain et al., 2022), weakened the nocturnal barrier to fire spread (Balch et al., 2022), and contributed to more severe fire events in boreal and temperate biomes

(Cunningham et al., 2024; Jones et al., 2024). As fires increasingly extend into regions with high fuel loads, global fire emissions have remained relatively stable despite the overall decline in burned area (van der Werf et al., 2025). Meanwhile, expanding human settlement near wildlands (Schug et al., 2023) has increased the extent of the wildland-urban interface (WUI) (Chen et al., 2024; Guo et al., 2024; Tang et al., 2024), thereby increasing human exposure to wildfires (Teymoor Seydi et al., 2025) and wildfire smoke–related premature mortality (Zhao et al., 2025). Assessing these evolving fire regimes and their societal and environmental impacts requires long-term, internally consistent global fire emissions datasets.

Near-real-time (NRT) fire emissions products are critical for the timely assessment of fire impacts on atmospheric chemistry and air quality, rapid response to evolving fire disasters, and the placement of such events in the context of the historical record. Several widely used operational NRT systems rely primarily on fire radiative power (FRP) observations from geostationary (GEO) and low Earth orbit (LEO) satellites. For example, the Copernicus Atmosphere Monitoring Service (CAMS) Global Fire Assimilation System (GFAS) (Kaiser et al., 2012) and NASA's Quick Fire Emissions Dataset (QFED) (Darmenov & da Silva, 2015) estimate emissions based on active fire detections from the Moderate Resolution Imaging Spectroradiometer (MODIS) sensors, with calibrations tied to external inventories or constrained by atmospheric observations. The Fire INventory from NCAR (FINN) (Wiedinmyer et al., 2011, 2023) provides fire emissions estimates derived from land cover data and active fires, supporting regional air quality applications. Similarly, NOAA's Hazard Mapping System (HMS) (Schroeder et al., 2008), the Blended Global Biomass Burning Emissions Product (GBBEPx) (Zhang et al., 2012; Li et al., 2022) and the HRRR-Smoke model (Ahmadov et al., 2017) integrate observations from multiple satellite sensors to improve detection and emissions quantification. These systems provide indispensable datasets for NRT monitoring and forecasting, but further efforts are needed to ensure consistency with long-term historical records.

The Global Fire Emissions Database (GFED) is a suite of gridded datasets that provide global estimates of burned area and associated emissions of gases and aerosols from landscape fires. Burned area estimates in GFED are primarily derived from satellite observations of surface reflectance change and the delineation of fire-affected areas. GFED emissions calculations follow the Seiler and Crutzen (1980) framework, combining burned area with fuel consumption estimates from a biogeochemical model and emission factors derived from laboratory and field measurements. GFED has undergone several iterations, resulting in multiple versions that progressively refine burned area and emissions (Chen et al., 2023; Giglio et al., 2006, 2010; Randerson et al., 2012; van der Werf et al., 2006, 2010, 2017). The most recent release, GFED version 5 (GFED5) (van der Werf et al., 2025), improves burned area estimates by accounting for small fires undetected by moderate-resolution sensors (Chen et al., 2023) and by incorporating higher-resolution imagery and a cropland-specific methodology to better represent agricultural burning (Hall et al., 2024). The full GEED5 product covers the 1997-2022 period. The core emissions model uses multiple 500-m MODIS products to track the temporal evolution of aboveground and surface fuels across ecosystems, with explicit treatment of deforestation and peat fires (van Wees et al., 2022). Emission factors draw upon an extensive compilation of field and laboratory measurements, including aircraft observations from recent field campaigns (Binte Shahid et al., 2024). Interannual variability over 1997-2022 is substaintial in this record (Table S1), with global burned area from GFED5 ranging from 620 to 920 million hectares per year (Mha yr^{-1}) and fire emissions ranging from 2.9 to 4.4 petagrams of carbon per year (Pg C yr^{-1}). Across GFED versions, mean global annual burned area over this period ranges from 340 to 780 Mha yr^{-1}, while mean annual fire emissions range from 2.0 to 3.4 Pg C yr^{-1}, reflecting differences in input datasets and methodological choices.

While GFED has provided essential retrospective data for understanding fire impacts on the Earth system, reducing data latency to support NRT applications remain a priority. However, the MODIS instruments aboard NASA's Terra and Aqua satellites, which provide core data for many global fire burned area and emissions datasets, are aging and have experienced orbital drift that has substantially altered their local overpass times (Loeb et al., 2024; Parkinson, 2022). The GEED5 dataset ends in 2022, when orbital drift-induced changes surpassed the thresholds defined for high-quality science products. The Visible Infrared Imaging Radiometer Suite (VIIRS) instruments on multiple NASA and NOAA satellites offer many of the same capabilities as MODIS and are widely considered a viable continuity data source for MODIS-based land products (Román et al., 2024; Giglio et al., 2025). Here, we present a system for generating GFED5-compatible NRT global burned area and emissions datasets for the post-MODIS era using 375-m VIIRS active fire detections (Fig. 1). We are motivated by the urgent need to quantify recent fire extremes and place their magnitudes in the context of the GFED5 global record. This work represents a first step toward developing global fire records that merge VIIRS and MODIS observations, prior to a more comprehensive fusion of science-quality burn area time series from the two sensors, which remains a key priority but requires further investment. Our approach (Fig. 2) uses a two-step scaling framework. First, daily VIIRS active fire counts are converted to burned area using region- and biome-specific effective fire areas (burned area per active fire) derived from GFED5. Second, burned area is translated into emissions using fuel consumption lookup tables constructed from GFED5 burned area and emissions as a function of fire type and continental-scale region. This framework features several novel aspects: (1) joint estimation of burned area and emissions through a unified scaling approach; (2) classification of fires into 16 broad ecosystem types to support biome-specific analyses; and (3) contextualization of recent fire activity within a long-term, internally consistent global fire record.

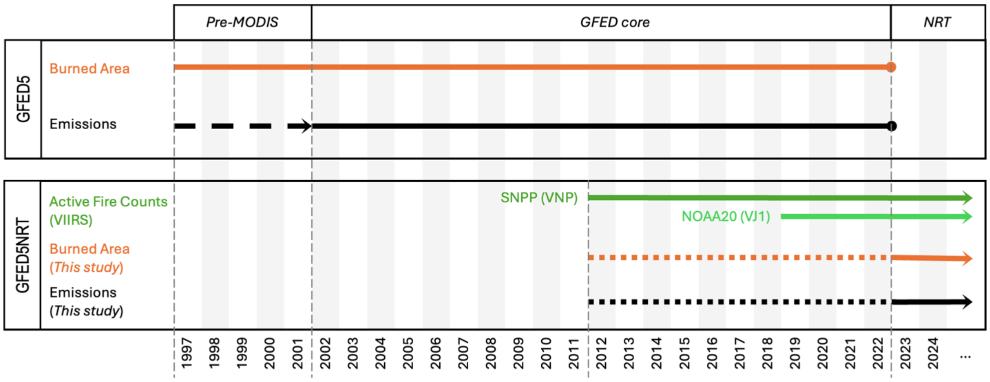

Figure 1. Timelines of GFED5NRT products and primary input datasets. Layers shown include VIIRS active fire counts, burned area, and fire emissions. Dashed lines for GFED5 indicates the pre-MODIS period, when data were reported at coarser spatial resolution. Dotted lines for GFED5NRT denote the periods used for data calibration and for deriving scaling coefficients.

We applied the scaling algorithm to daily VIIRS active fire detections from the NOAA/NASA Suomi-NPP (SNPP) and NOAA-20 satellites, generating two independent time series of burned area and emissions estimates with minimal latency. To reduce biases associated with oblique viewing geometry and data gaps caused by intermittent instrument outages, we merged these streams to produce the combined GFED5 near-real-time extension (GFED5NRT). GFED5NRT extends the temporal coverage of GFED5, providing characterization of fire activity, burned area, and associated emissions during the post-MODIS era, as well as more timely documentation of recent extreme wildfire events. We developed a Python-based processing system that automatically retrieves VIIRS NRT active fire data from NASA's Fire Information for Resource Management System (FIRMS), applies corrections for viewing geometry and data gaps, and uses pre-calculated region- and biome-specific scaling coefficients to estimate daily burned area and emissions operationally. By combining contemporary satellite observations with a consistent scaling framework, GFED5NRT provides temporally consistent and reliable estimates of burned area and emissions across fire types, supporting both retrospective analyses of fire variability and NRT monitoring of ongoing fire activity.

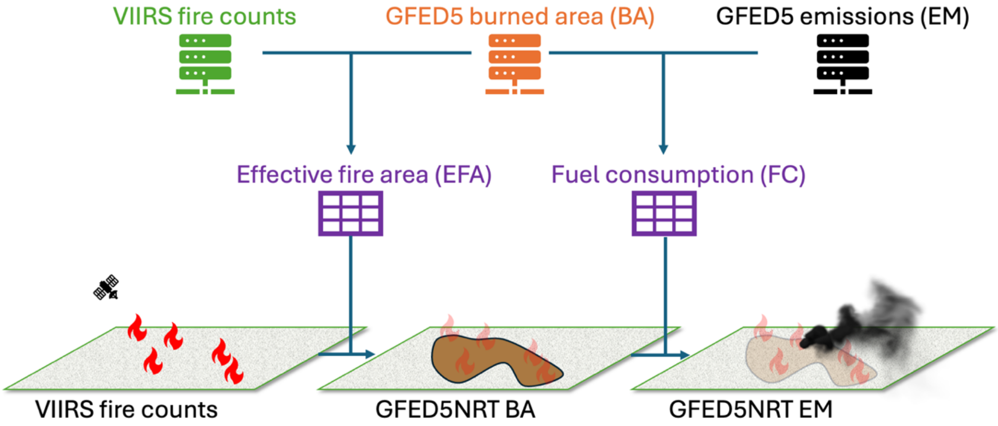

Figure 2. Schematic of the two-step scaling approach used to generate the GFED5NRT global burned area (BA) and fire emissions (EM) datasets from VIIRS active fire counts. Two biome-specific scaling factors—effective fire area (EFA; burned area per fire count) and fuel consumption (FC; carbon emissions per unit burned area)—were derived for each region by linking VIIRS active fire detections to the GFED5 data.

2. Data and Method

2.1 GFED5 burned area and emissions

The GFED5 burned area dataset was developed by integrating multiple remote sensing data streams (Chen et al., 2023). It builds primarily on the MODIS burned area time series (Giglio et al., 2018; Justice et al., 2002). To reduce commission errors associated with the coarse spatial resolution of MODIS (500 m), burned area estimates were calibrated using higher-resolution (20-30 m) observations from Landsat and Sentinel-2. Burned areas not detected by MODIS were further used to quantify these small fires, with MODIS active fire detections serving as a proxy for their occurrence. Agricultural burned area was further updated using the global cropland-focused burned area product GloCAB (Hall et al., 2024). GFED5 provides global monthly burned area estimates at 0.25° spatial resolution, with attribution by ecosystem and fire type.

In van der Werf et al. (2025), a slightly modified version of the methodology described in Chen et al. (2023) was implemented to estimate GFED5 burned area (version 5.1) through 2022. GFED5 emissions were calculated using this burned area dataset in the classical framework of Seiler and Crutzen (1980). For each 0.25° grid cell, emissions of individual species were estimated as the product of burned area, fuel consumption (defined as fuel load multiplied by combustion completeness), and species-specific emission factors that convert dry matter burned to chemical species. Fuel consumption was derived using the Carnegie-Ames-Stanford Approach (CASA) biogeochemical model (Potter et al., 1993) and further constrained by multiple observational datasets (van Wees et al., 2022). Monthly emissions were temporally disaggregated to daily and hourly scales using active fire detections from a combination of polar-orbiting and geostationary satellites to capture sub-monthly variability in fire activity (Mu et al., 2011). The GFED5 burned area and emissions datasets (version 5.1) are publicly available at www.globalfiredata.org.

The gridded, fire-type-specific GFED5 data cover the core MODIS era from 2002 to 2022. As described in Chen et al. (2023) and van der Werf et al. (2025), GFED5 was also extended to the pre-MODIS period (1997–2001) using active fire detections from the Visible and Infrared Scanner (VIRS) aboard the Tropical Rainfall Measuring Mission (TRMM) and the Along Track Scanning Radiometers (ATSR) flown on multiple platforms. For this earlier period, the dataset was produced at a coarser 1° spatial resolution and does not distinguish among land cover types.

Throughout this paper, GFED5 refers to the updated version 5.1 burned area and emissions datasets described in van der Werf et al. (2025), including the pre-MODIS period (Fig. 1). These standard products are used during the overlap period with VIIRS (2012-2022) to derive scaling coefficients that convert VIIRS active fire counts to burned area and emissions for the near-real-time product (Fig. 2).

2.2 VIIRS active fire data

VIIRS is a multi-band imaging instrument that collects imagery and radiometric measurements across visible and infrared wavelengths, enabling the detection of thermal anomalies associated with landscape fires and other heat sources. Compared with MODIS (1 km), the finer spatial resolution of VIIRS (375 m) provides more accurate fire location information and higher detection efficiency, thereby improving fire mapping, fire behavior characterization, and applications in disaster response and land management. Unlike MODIS, however, VIIRS lacks a mid-morning (10:30 local time) overpass, which may lead to the underdetection of fires with pronounced diurnal variability in activity.

The NASA VIIRS 375-m thermal anomalies and active fire products are distributed as both science-quality data (Schroeder et al., 2024) and NRT data. The science-quality datasets are quality-controlled and internally consistent, with a primary objective of supporting long-term climate research, but data latency is typically several months. In contrast, the NRT data stream is available within hours of observation, making it better suited for operational decision support and early warning applications.

In this study, we obtained the science-quality VIIRS 375 m fire location products (VNP14IMGML and VJ114IMGML, Collection 2 version 4) from the University of Maryland Fuoco SFTP server (fuoco.geog.umd.edu). These data from 2012 to 2022 were used to train the scaling model that convert active fire counts to burned area and fire emissions. To generate the GFED5NRT product, we used VIIRS NRT active fire data available through NASA LANCE FIRMS. As discussed below, we selected the NRT fire image products (VNP14IMG_NRT and VJ114IMG_NRT), rather than the NRT fire location products, to enable viewing-angle corrections (Sect. 2.3.3).

VIIRS instruments are currently carried on three satellites in the Joint Polar Satellite System (JPSS): SNPP, NOAA-20, and NOAA-21. Their orbital configuration allows each satellite to observe a given location at approximately the same local solar time, but from different viewing angles. Merging VIIRS observations across platforms has been shown to reduce artificial day-to-day variability and biases associated with changing viewing geometry (Giglio et al., 2025). In this study, we integrated VIIRS active fire observations from the SNPP and NOAA-20 to balance the need for a consistent historical record with continuity for future extensions of the GFED5NRT product. To further reduce biases arising from day-to-day variations in sensor viewing geometry, we additionally generated a GFED5NRT data layer that combines observations from both satellites, taking advantage of their deliberate orbital phasing.

2.3 Active fire recording and adjustments

2.3.1 Active fire counts

To ensure consistency with the fire-type classification and grid structure of standard GFED5, VIIRS active fire detections were aggregated by land cover class by overlaying fire centroids onto 500-m land cover maps. An annual land cover type was assigned to each 500-m MODIS sinusoidal grid cell (van Wees et al., 2022) using an integrated dataset combining the MODIS MCD12Q1 Collection 6.1 land cover product (Friedl & Sulla-Menashe, 2019), a tropical peatland map (Gumbricht et al., 2017), and a fire-persistence-based deforestation mask (Chen et al., 2023). A total of 16 land cover classes were defined, including 13 standard biome types and three special burning types: deforestation, peatland, and agricultural burning. In each 0.25° grid cell, active fire detections were aggregated across these classes, ensuring consistency with the burned area and emissions stratification applied in GFED5 (Table 2 of van der Werf et al., 2025). To minimize the effects of VIIRS sampling biases and retrieval uncertainties, additional corrections were applied prior to the estimation of burned area and emissions, as described in the following sections.

2.3.2 Static hotspot filtering

The VIIRS science-quality active fire products classify detected thermal anomalies into several categories, including vegetation fires, active volcanos, offshore detections, and other static land heat sources. In contrast, the VIIRS NRT active fire products do not explicitly separate vegetation fires from persistent non-vegetation thermal sources. To address this limitation, we developed a static hotspot mask that combines two complementary sources of information. This mask has a spatial resolution of 0.01° × 0.01°.

First, a hotspot-based static mask was constructed using historical SNPP VIIRS observations from 2012-2022 to identify 0.01° grid cells with more than five detections classified as non-vegetation fires (type $\neq 0$). Second, a report-based static mask was compiled from documented locations of persistent thermal sources, including gas flares, landfills, volcanoes, solar power facilities, power plants, and refineries (see SI Text S1). These two components were combined to produce a comprehensive static hotspot mask that removes presumed non-vegetation thermal anomalies from the VIIRS NRT data, thereby improving the accuracy of fire detection and subsequent burned area and emissions estimates in GFED5NRT.

2.3.3 VIIRS viewing geometry adjustment

Each VIIRS active fire detection is associated with a specific scan angle, identified by the sample number in the science-quality VIIRS active fire location files. Detection efficiency varies with scan angle due to factors such as pixel size, canopy height, illumination geometry, atmospheric attenuation, and filtering by the retrieval algorithm. While these effects largely average out over monthly time scales, they can introduce significant biases in daily burned area and emission estimates (Giglio et al., 2025).

To correct for this, we developed scan-angle-specific lookup tables using the full set of standard VIIRS active fire detections from SNPP during 2019–2021. Fire counts were stratified by cross-track sample number (0–6399), day/night status, month, and dominant land cover type within 0.25° grid cells (see SI Text S2). Weighting factors were derived for each sample bin based on total fire counts, removing scan angle dependence while conserving the total fire radiative power across all sample numbers (Fig. S1). This ensures that total emissions estimates remained unchanged. The resulting weighting factors were applied to individual VIIRS detections, and the corrected fire counts were aggregated by land cover type within each 0.25° grid cell.

Scan angle information is only available in the science-quality product (VNP14IMGML and VJ114IMGML) and is absent in the NRT fire location products (VNP14IMGDL_NRT, VJ114IMGDL_NRT). To address this limitation, we used upstream two-dimensional NRT imagery products (VNP14IMG_NRT, VJ114IMG_NRT) to generate daily fire location files in a VNP14IMGDL_NRT-like format, incorporating both sample numbers and key fire attributes. These additional files were then used to perform viewing geometry correction and normalize fire counts.

2.3.4 Adjustment of fire counts in deforestation areas

VIIRS active fire detections were aggregated by land cover type within each 0.25° grid cell, with individual detections assigned to land cover classes at 500-m resolution. In near-real-time applications, instantaneous land cover data are often unavailable, and the most recent available year of land cover information from the MODIS MCD12Q1 product is therefore used. However, in regions undergoing rapid deforestation, this temporal mismatch can lead to substantial misclassification: fires associated with recent forest loss may be missed, while unrelated fires may be incorrectly attributed to deforestation, resulting in biased emissions estimates.

To mitigate this issue, VIIRS active fire counts were adjusted by assuming temporal stability in the monthly fraction of deforestation-related burning within 0.25° tropical deforestation grid cells. Climatological monthly fractions of deforestation-related fire counts, averaged over 2013–2022, were first calculated for each grid cell. These fractions were then applied to the total VIIRS active fire counts to derive adjusted estimates of deforestation-related fire activity. Fire counts associated with other land cover types were scaled proportionally to conserve the total number of detections.

2.4 Estimating burned area and emissions from active fire counts

We applied a two-step scaling approach (Fig. 2) to convert VIIRS active fire counts, stratified into 16 land cover types at 0.25° resolution, into global burned area and fire emissions estimates.

In the first step, biome-specific scaling factors, termed effective fire area (EFA) scalars, were derived for multiple geographical regions by relating science-quality VIIRS active fire detections to GFED5 burned area data during the MODIS-VIIRS overlap period (2012–2022). Only detections classified as vegetation fires (fire type code = 0) were used in deriving EFA. EFA represents the mean burned area (km^2) per active fire detection for each region and land cover type.

We evaluated a suit of aggregation schemes (SI text S3; Table S2) that varied in spatial scale (0.25° grid cell, GFED region, or global), temporal resolution (annual or monthly), and treatment of land cover (lumped or type-specific). Based on overall performance across statistical metrics, including bias, correlation coefficient, normalized root mean square error (Table S3), as well as aggregation efficiency (Table S2), we selected region- and land cover-specific EFA scalars associated with the *Regftp* scheme. In this scheme, active fires are aggregated within each GFED region and land cover type (Tables S2). These scalars were used to generate GFED5NRT. In principle, the *Regftp* scheme could yield up to 224 EFA scalars globally, from the product of 14 continental regions and 16 burning types; in practice, however, not all burning types occur in every region.

The optimized EFA scalars were subsequently applied to VIIRS active fire counts to generate the GFED5NRT burned area product for years following the GFED5 record (1997-2022). Beginning in 2023, daily VIIRS active fire counts by land cover type were multiplied by corresponding EFA scalars to estimate burned area at 0.25° resolution.

In the second step, we constructed a fuel consumption (FC) look-up table based on historical GFED5 burned area and emissions data. Using the same aggregation strategy as for EFA, we derived region- and biome-specific FC scalars, which were then applied to convert GFED5NRT burned area into emissions for each burning and or land cover type. Several major land cover types exhibited pronounced long-term trends in FC during 2002-2022. To partially account for these trends, mean FC values from the more recent 2013–2022 period were used to estimate GFED5NRT emissions beyond 2022. Emissions of trace gases and aerosols were derived using the same emission factors as in the core GFED5 data, and using a gridded (0.25 degree) daily climatology for spatiotemporally variable savanna emission factors of CO_2, CO, CH_4, and N_2O (Vernooij et al., 2023) based on the 2002-2022 time series.

2.5 Generating the GFED5NRT products

To support the operational, near-real-time production of daily GFED5NRT datasets, we developed a fully automated, standalone software system that implements the complete processing workflow (Fig. S2). The system is built primarily in Python and is distributed with all required ancillary inputs, including precomputed lookup tables and configuration files, allowing the pipeline to run independently without manual preparation. The workflow comprises sequential modules for automated acquisition of VIIRS active fire data, screening and filtering of detections, conversion of fire counts to burned area, and generation of corresponding emissions estimates. Execution of the workflow is managed by a master shell script, which is scheduled to run daily via a cron job. Upon execution, the script retrieves the latest VIIRS data from the FIRMS server, verifies global data completeness, and initiates GFED5NRT production only when sufficient coverage is available, thereby enabling robust and timely updates with minimal user intervention.

Using this automated framework, daily GFED5NRT products are routinely generated with latencies of only a few hours. Three NRT product variants are produced: one based exclusively on SNPP VIIRS observations, one based on NOAA-20 VIIRS observations, and a combined product. In the combined product, burned area and emissions within each grid cell are calculated as the arithmetic mean of the SNPP- and NOAA-20-based estimates when both instruments are operating nominally. If observations from one satellite are unavailable, the combined product defaults to the remaining instrument. On days when active fire data are missing from both satellites, GFED5NRT production is suspended for that date. Each daily product is distributed in two compact NetCDF files: species files, which report emissions of individual trace gas and aerosol species, and ecosystem files, which describe the allocation of burned area and carbon emissions across the 16 land cover and burning classes. File structure, variable naming, and metadata conventions are fully consistent with those of the standard GFED5 products.

When science-quality VIIRS active fire location data become available from the Fuoco server, the system will rerun the scaling procedure using these higher-quality inputs. During reprocessing, non-vegetation thermal anomalies are excluded directly using the fire *type* flag (type $\neq$ 0) provided in the science-quality data, and viewing geometry corrections are applied based on the *sample* column information in the same files. Dates with missing observations for individual VIIRS instruments, as documented on the FIRMS missing-dates webpage and summarized in Table S4, are filled using temporal interpolation. As science-quality data become available on an irregular schedule, the reprocessed GFED5NRT datasets are updated episodically for the SNPP-only, NOAA-20-only, and combined products. The daily datasets are subsequently aggregated to monthly products to facilitate analysis. Unless otherwise noted, all results presented in this study are based on the reprocessed, science-quality GFED5NRT combined product. For evaluation purposes, additional science-quality-based GFED5NRT burned area estimates derived solely from SNPP observations were generated for the 2012–2022 period.

2.6 Data for GFED5NRT evaluation

We assessed the performance of the GFED5NRT burned area and fire emissions products using a diverse set of independent global and regional reference datasets.

Evaluation of burned area focused on retrospective comparisons in Canada and South America, where high-quality regional products are available. For South America, we used the INPE AQ1km burned area dataset (https://terrabrasilis.dpi.inpe.br/queimadas/aq1km/), which is derived from MODIS 1-km imagery in combination with active fire detections from multiple satellite platforms (Libonati et al., 2015), as well as the MapBiomas Fire product (Collection 4; https://brasil.mapbiomas.org/en/mapbiomas-fogo/), which is based on 30-m Landsat imagery and a machine-learning classification framework (Alencar et al., 2022). For Canada, we employed the Canadian National Fire Database (CNFDB, https://cwfis.cfs.nrcan.gc.ca/ha/nfdb), which compiles fire perimeter records reported by provincial and territorial fire management agencies, and the National Burned Area Composite (NBAC; https://cwfis.cfs.nrcan.gc.ca/datamart/metadata/nbac), a Landsat-based burned area product generated using change-

https://doi.org/10.5194/essd-2026-158
Preprint. Discussion started: 31 March 2026

detection techniques. In addition, two independent estimates of total burned area in Canada for 2023 were used for benchmarking purposes: NRCan_2023, derived from Natural Resources Canada Fire M3 hotspot-based fire perimeters, and TIIC_2023, produced using the Tracking Intra- and Inter-year Change (TIIC) algorithm (Pelletier et al., 2024).

For evaluation of fire emissions, daily GFED5NRT carbon monoxide (CO) emissions for 2023 were compared against three widely used global fire emissions inventories: the Fire Inventory from NCAR (FINN, version 2.5; Wiedinmyer et al., 2023), the Blended Global Biomass Burning Emissions Product (GBBEPx, version 3; Li et al., 2022), and the CAMS Global Fire Assimilation System (GFAS, version 1.2; Kaiser et al., 2012).

3. Results

3.1 Effective fire area and fuel consumption

The GFED5NRT burned area (BA) and fire emissions (EM) products were derived from VIIRS active fire counts using two primary scaling coefficients: EFA and FC. Aggregated over the calibration period (2012-2022), EFA was calculated as the ratio of BA to the number of active fire detections, representing the mean burned area associated with a single VIIRS active fire detection, while FC was calculated as the ratio of EM to BA, reflecting the mean carbon emissions per unit burned area.

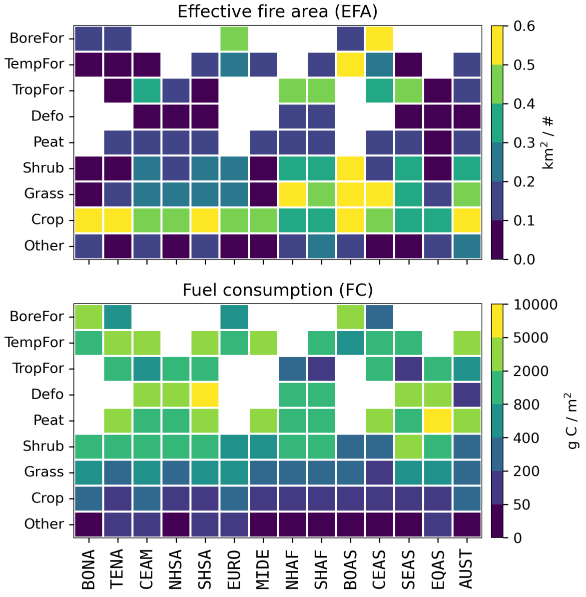

Figure 3. Mean EFA and FC by GFED region and aggregated land cover type. These scaling coefficients were derived from VIIRS active fire counts and GFED5 burned area and emission data for 2012-2022. Land cover classes based on GFED5 burned area classifications (Table 2 in *van der Werf et al.*, 2025) were consolidated into nine groups: **BoreFor** ('*Boreal forest*', '*Sparse boreal forest*', and '*Tundra*'); **TempFor** ('*Temperate forest*'); **TropFor** ('*Tropical forest*'); **Defo** ('*Deforestation*'); **Peat** ('*Peatland*'); **Shrub** ('*Temperate shrubland*', '*Temperate mosaic*', '*Tropical shrubland*', and '*Woody savanna*'); **Grass** ('*Temperate grassland*', '*Tropical grassland*', and '*Open savanna*'); **Crop** ('*Cropland*'); and **Other** (all remaining burning types).

As shown in Fig. 3, both EFA and FC exhibit substantial variability across land cover types and geographic regions. On average, EFA values are higher in grasslands and shrublands than in forests, reflecting differences in fire behavior and detection efficiency. The contrast arises from slower fire spread and more persistent burning within forests, combined with under-detection of fast-moving fires in grassland and shrublands. Exceptionally low EFA values occur in tropical peatlands and deforested regions, where high fuel loads and prolonged smoldering combustion result in repeated active fire detections over relatively small areas. In contrast, croplands exhibit the highest EFA values among all land cover types, suggesting that agriculture burning is frequently under-detected, due to short fire duration, small fire size, low fire intensity, or burning that occurs between VIIRS overpasses (Hall et al., 2016, 2024).

Fuel consumption varies systematically by land cover type, consistent with differences in average fuel availability and biomass density. FC generally decreases from forests to shrublands, grasslands, and croplands, reflecting the declining gradient in ecosystem biomass. Across most GFED regions, FC values are relatively consistent, with notable exceptions including elevated FC for peatland fires in Equatorial Asia (EQAS) and deforestation fires in southern-hemisphere South America (SHSA).

3.2 Evaluation of GFED5NRT

Compared with GFED5, the GFED5NRT monthly time series of burned area and emissions exhibit similar temporal behavior across all GFED regions, capturing both seasonal cycles and interannual variability (Fig. 4). Comparisons of annual burned area at 0.25° resolution during 2012-2022 (Fig. S3) demonstrate strong spatial agreement between the two products. To further assess consistency, we compared monthly latitudinal zonal anomalies of burned area and emissions—normalized as Z-scores—between GFED5 and GFED5NRT using Hovmöller diagrams (Fig. 5). The close correspondence of anomaly structures, together with the smooth transition from the GFED5 period (2012–2022) to the GFED5NRT period (2023–2024), indicates strong internally consistency between the two datasets at large spatial scales.

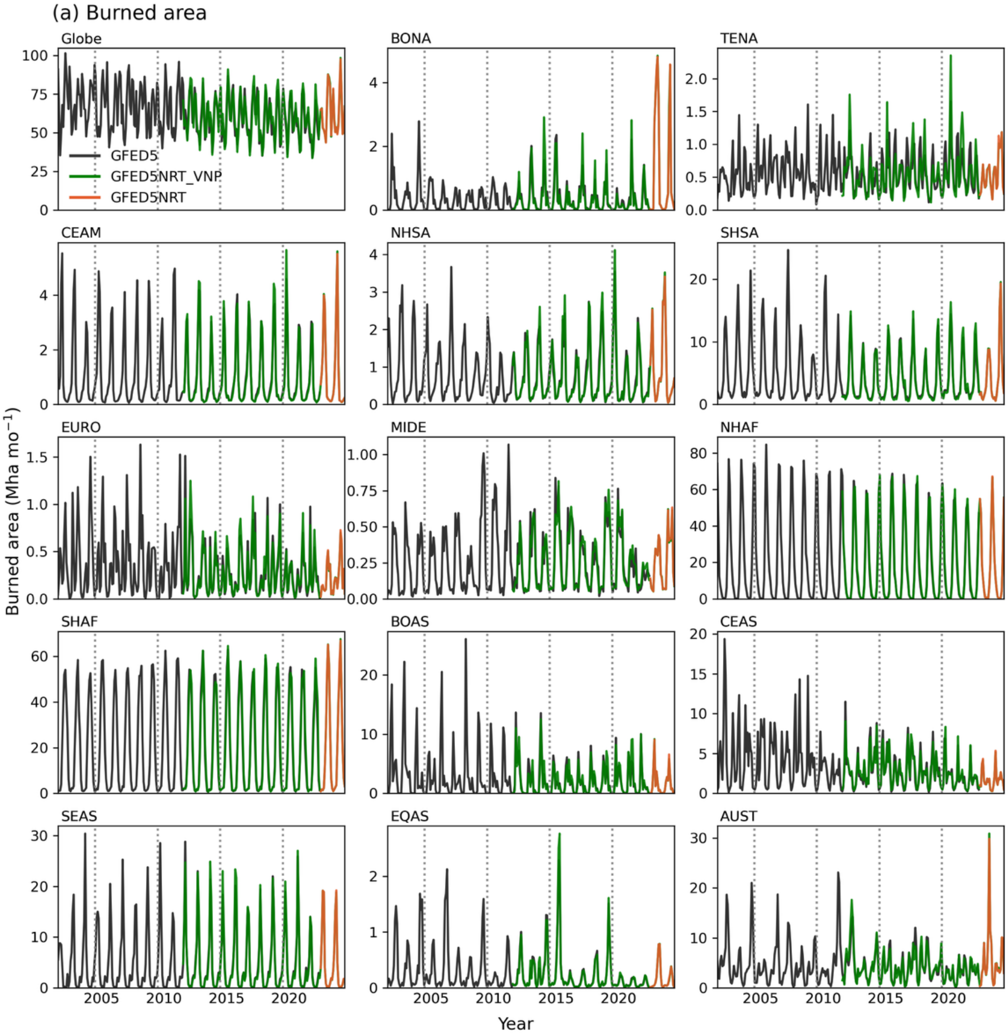
(a) Burned area

https://doi.org/10.5194/essd-2026-158
Preprint. Discussion started: 31 March 2026

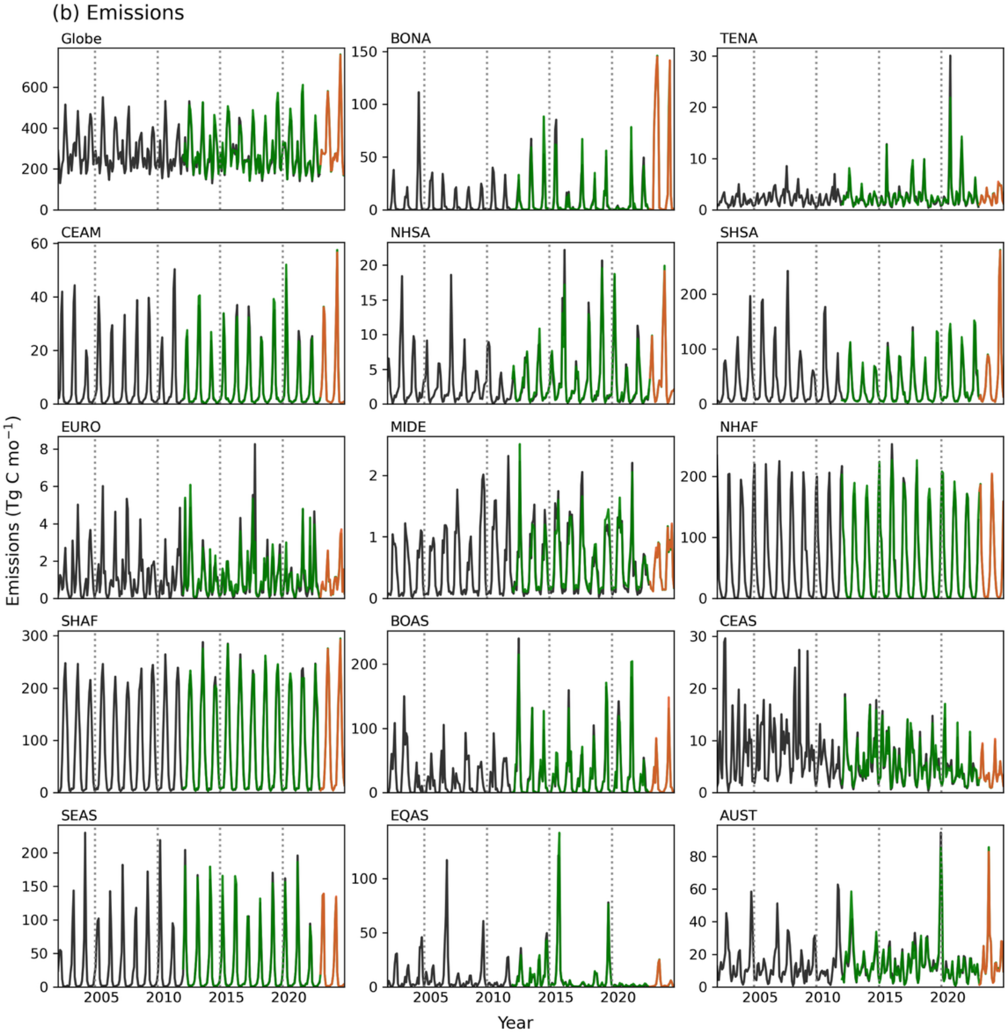

Figure 4. Monthly time series of regionally summed (a) burned area (Mha mo^{-1}) and (b) fire emissions (Tg C mo^{-1}) from GFED5 (2002-2022; black lines) and GFED5NRT (derived from SNPP and NOAA-20 combined, 2023-2024; orange lines). For comparison, the time series of GFED5NRT derived using SNPP only (GFED5NRT_VNP, 2012-2024; green lines) is also shown.

336

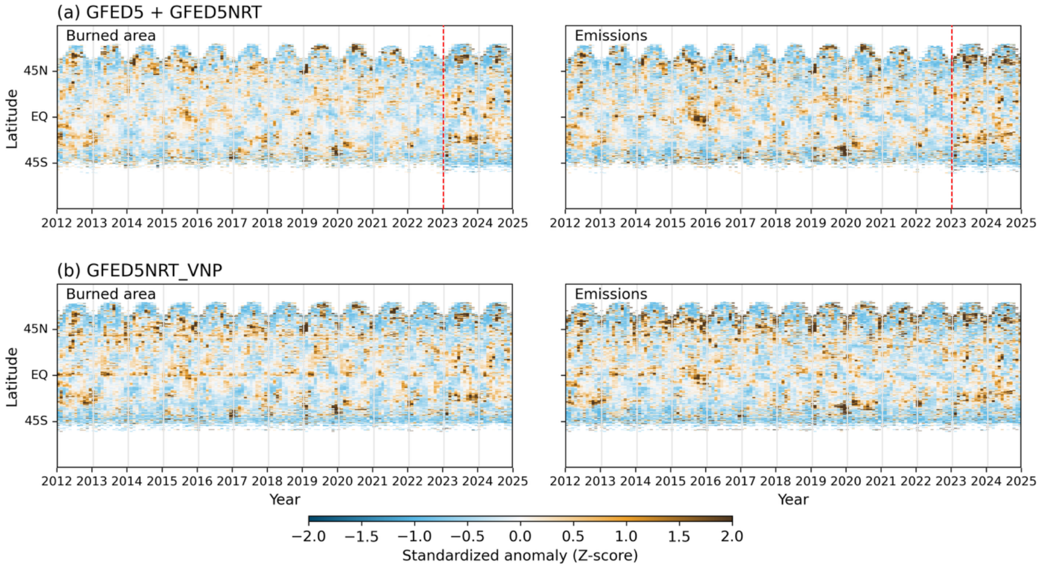

Figure 5. Monthly Z-score of burned area (BA) and fire emissions (EM) in each 0.25° latitudinal band. (a) GFED5 (2012-2022) and GFED5NRT (SNPP and NOAA-20 combined version; 2023-2024); (b) GFED5ext derived using SNPP only (GFED5NRT_VNP) for 2012-2024. The unitless Z-score, or the normalized anomaly, is defined as Z = (*v*-*m*)/*std*, where *v* is the monthly burned area, *m* is the climatological monthly mean, and *std* is the standard deviation of interannual variability. The same climatological means and standard deviations from GFED5 (2012-2022) were used for the calculations of Z-scores in all three datasets.

The NASA VIIRS VNP64A1 burned area product, recently introduced as a successor to the long-term MODIS record, uses a modified mapping algorithm to provide global fire data continuity from 2012 into the coming decade (Giglio et al., 2025). Here we compare the GFED5NRT burned area estimates with VNP64A1. Overall, the spatial distribution of GFED5NRT burned area in 2023 shows moderate to good agreement with the VIIRS-based burned area product (Fig. S4), with GFED5NRT capturing more burned area associated with small fires.

When compared with independent burned area datasets derived from high-resolution satellite observations and regional fire records, total annual burned area estimates for Canada and Brazil from GFED5 and GFED5NRT are of comparable magnitude and exhibit similar interannual variability (Fig. S5). In Canada, GFED5 and GFED5NRT estimates are slightly higher than NBAC during extreme fire years (e.g., 2023 and 2024), likely because NBAC explicitly delineates small unburned islands that may not be resolved at coarser spatial resolutions. In Brazil, GFED5 and GFED5NRT totals generally agree with the INPE AQ1km product, but are substantially higher than MapBiomas, reflecting well-documented methodological differences among these datasets.

Finally, comparisons of daily carbon monoxide (CO) emissions in 2023 with three widely used global fire emissions inventories—FINN, GBBEPx, and GFAS—show that GFED5NRT captures similar day-to-day variability in global fire emissions (Fig. 6), although substantial regional differences remain in the absolute magnitude of emissions. These discrepancies underscore the importance of multi-dataset comparisons for uncertainty characterization, particularly when applying fire emissions products to air quality modeling, climate research, and carbon budget analyses.

https://doi.org/10.5194/essd-2026-158
Preprint. Discussion started: 31 March 2026

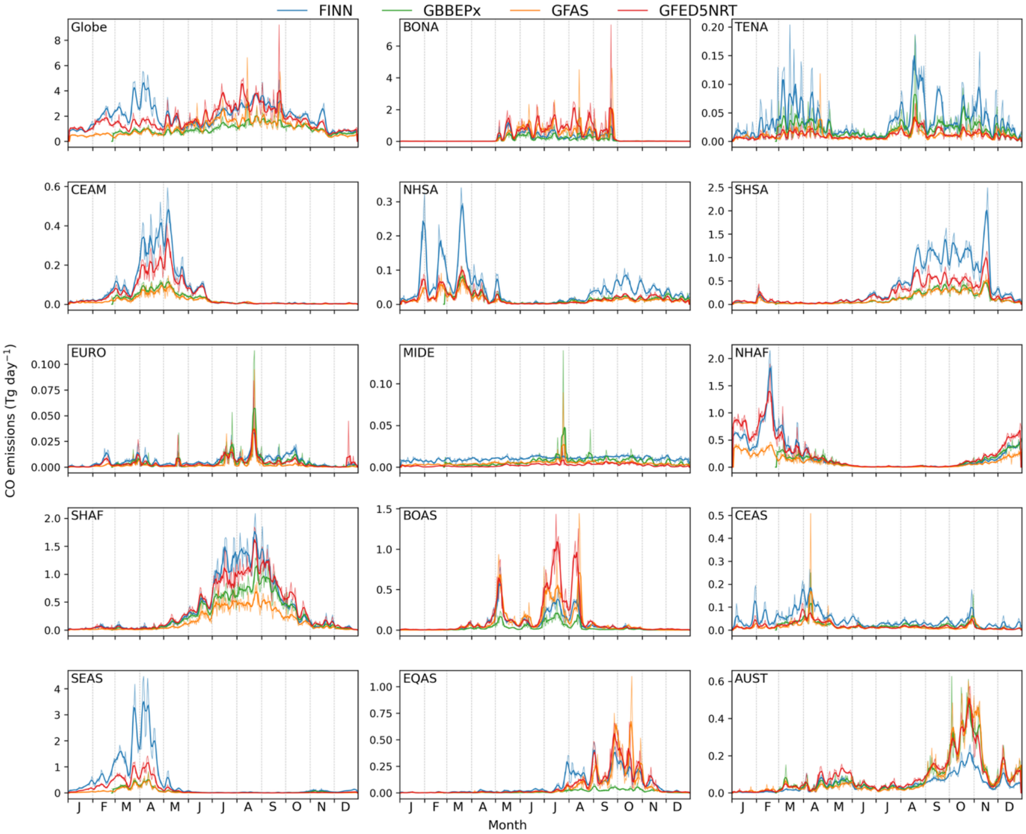

Figure 6. Comparison of daily global and regional CO emission totals in 2023 from GFED5NRT with three existing daily fire emissions datasets: the Fire Inventory from NCAR (FINN, v2.5), the Blended Global Biomass Burning Emissions Product (GBBEPx, v3), and the CAMS Global Fire Assimilation System (GFAS, v1.2). Light-colored lines show the original daily times series, and the dark-colored lines show the 5-day smoothed time series.

3.3 Fire burned area and emissions in 2023 and 2024

Based on GFED5NRT, global fire emissions are substantially elevated in both 2023 and 2024 relative to the GFED5 long-term mean for 2002-2022 (Figs. 7 and 8; Table S5). In 2023, the global total fire emissions (3.89 Pg C yr^{-1}) were anomalously high, driven by record-breaking emissions in boreal North America and positive anomalies in Central America, southern Africa, and Australia. In 2024, global fire emissions were even higher (4.03 Pg C yr^{-1}), reflecting a second consecutive year of extreme emissions in boreal North America, combined with pronounced positive anomalies in South America and southern Africa. Given that global fire emissions were relatively low in 2021 and 2022, the large positive wildfire emissions anomalies observed in subsequent years likely contributed substantially to the anomalously high atmospheric CO_2 growth rate observed during the 2023-2024 ENSO event (Friedlingstein et al., 2025).

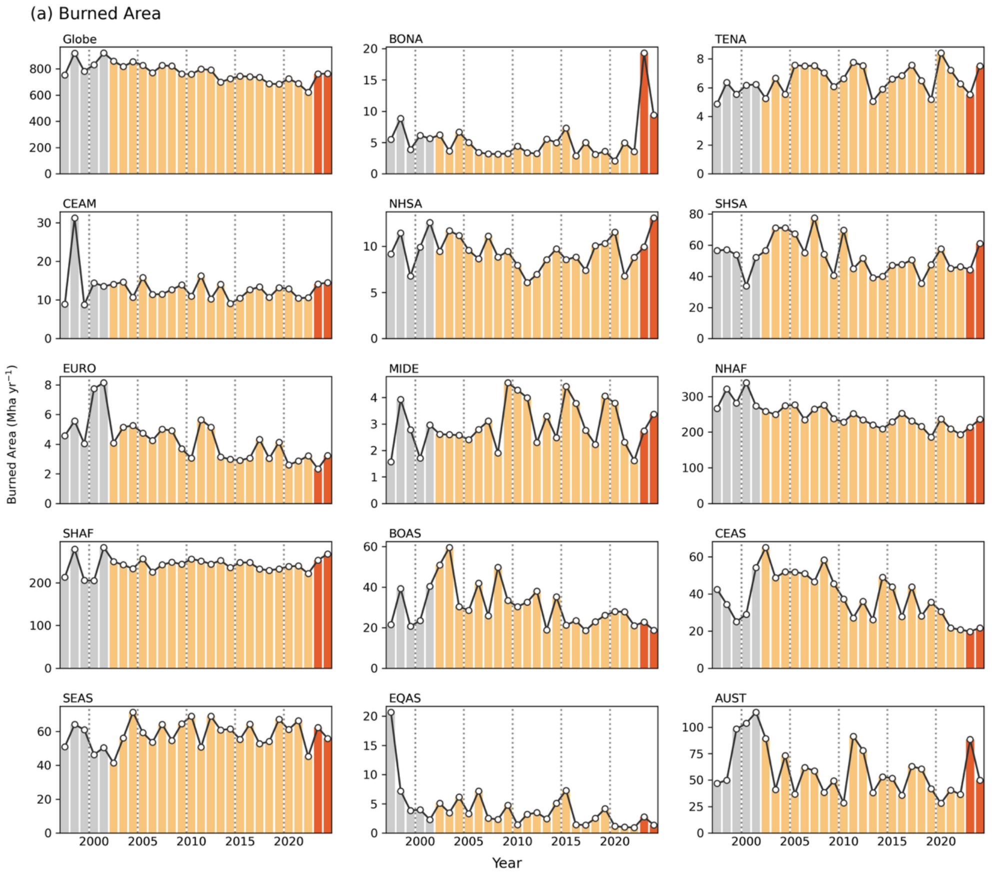
(a) Burned Area
Globe
BONA
TENA
CEAM
NHSA
SHSA
EURO
MIDE
NHAF
SHAF
BOAS
CEAS
SEAS
EQAS
AUST
Burned Area (Mha yr^{-1})
2000
2005
2010
2015
2020
Year

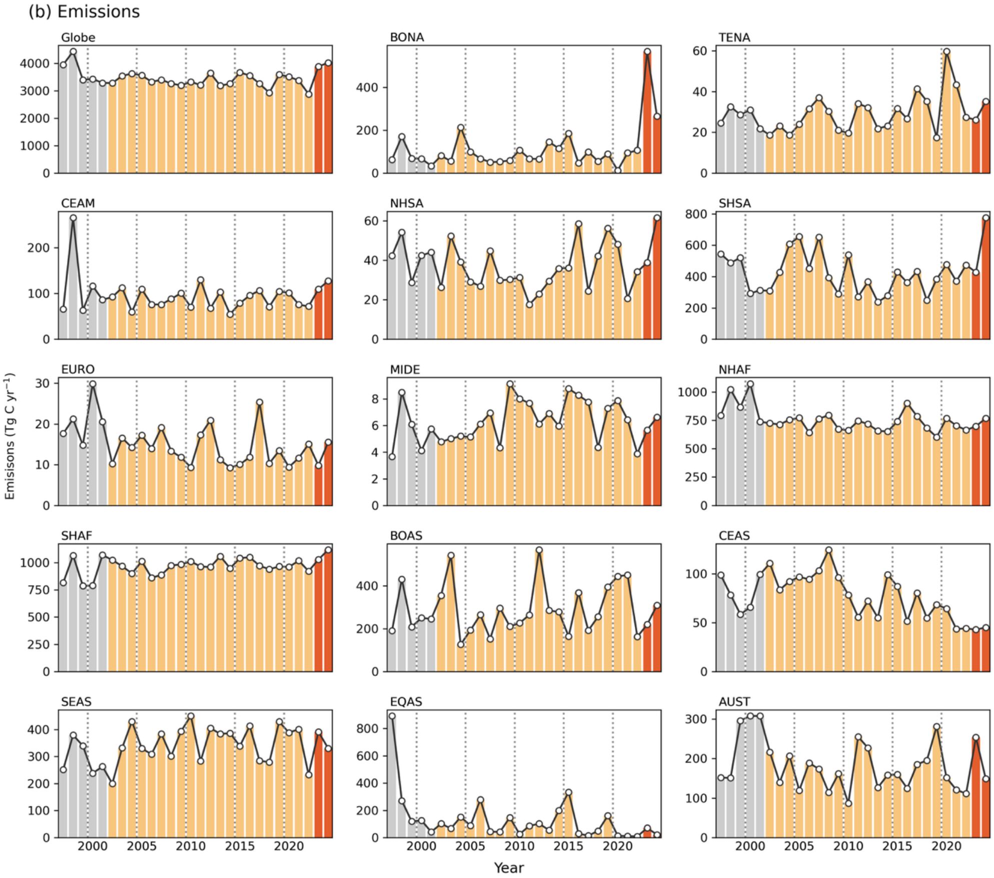

Figure 7. Extended annual time series of regionally summed (a) burned area (Mha yr^{-1}) and (b) fire emissions (Tg C yr^{-1}) from GFED5 for the core period (2002-2022, orange) and the pre-MODIS period (1997-2001, gray), along with the GFED5NRT product (2023-2024, red).

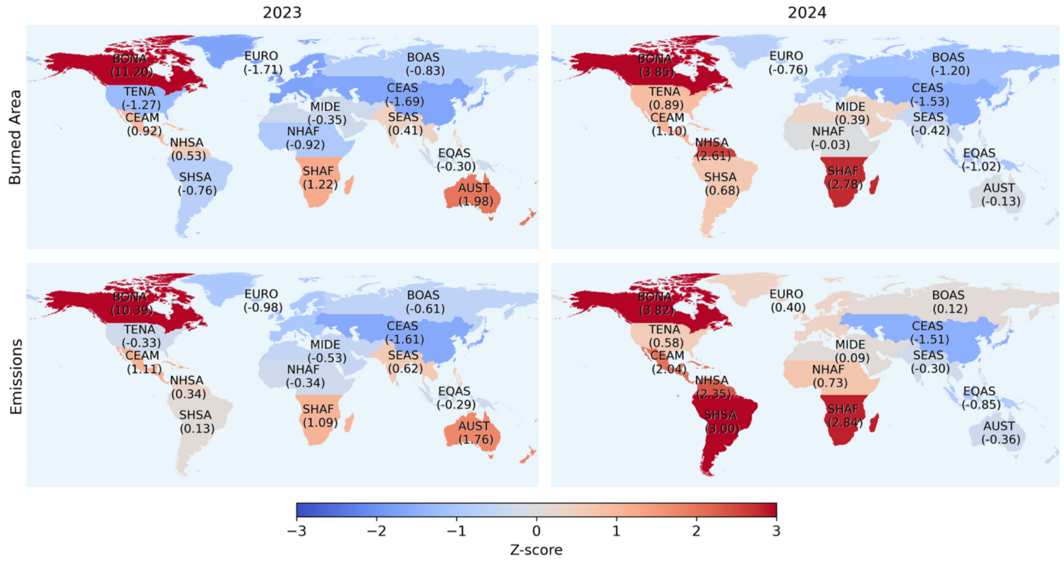

Figure 8. Global maps of Z-scores (standardized anomalies) for GFED5NRT burned area and fire emissions in 2023 and 2024. Red and blue colors indicate positive and negative anomalies, respectively. Numbers show the mean Z-scores (normalized using the GFED5 data during 2002-2022) for each of the 14 GFED regions.

At a global scale, the inclusion of two additional years of burned area observations from GFED5NRT weakens (but does not reverse) the long-term declining trend in burned area observed during the core GFED5 period (Table S5). This global decline is dominated by sustained reductions in burned area across northern Africa and boreal and central Asia (Fig. 7a). In these regions, burning levels in 2023 and 2024 from GFED5NRT are comparable to those observed near the end of the GFED5 record (2020–2022).

For emissions, the new GFED5NRT observations for 2023 and 2024 do not change the storyline reported by van der Werf et al. (2025) that there is no significant long-term trend in global carbon emissions from fires. Across regions, declining emissions trends in equatorial Asia, northern hemisphere Africa and central Asia are balanced by upward trends in boreal and temperate North America and southern hemisphere Africa. Within individual regions, a shift in fire activity toward ecosystems with higher fuel densities resulted in more positive trends in emissions than in burned area trends (Table S5).

3.4 Recent fire extremes

Fire activity exhibited significant spatial heterogeneity, even within individual GFED regions. GFED5NRT enables the timely identification of regional extreme fire hotspots and the characterization of fire behavior within these areas. Using Z-score based thresholds combined with spatial aggregation techniques (SI text S4), we identified 16 recent extreme fire events during 2023-2024 (Fig. 9) and quantified their emissions relative to the 2002–2022 climatology (Fig. S6). These events spanned multiple continents and were predominantly concentrated in tropical and boreal forests and shrublands. Collectively, the 16 events produced mean annual emissions of 1.9 Pg C during 2023–2024, which is about 0.8 Pg C (73%) above the 2002–2022 climatological average over the same regions (Table S6), accounting for more than half of global fire emissions during this biennial period.

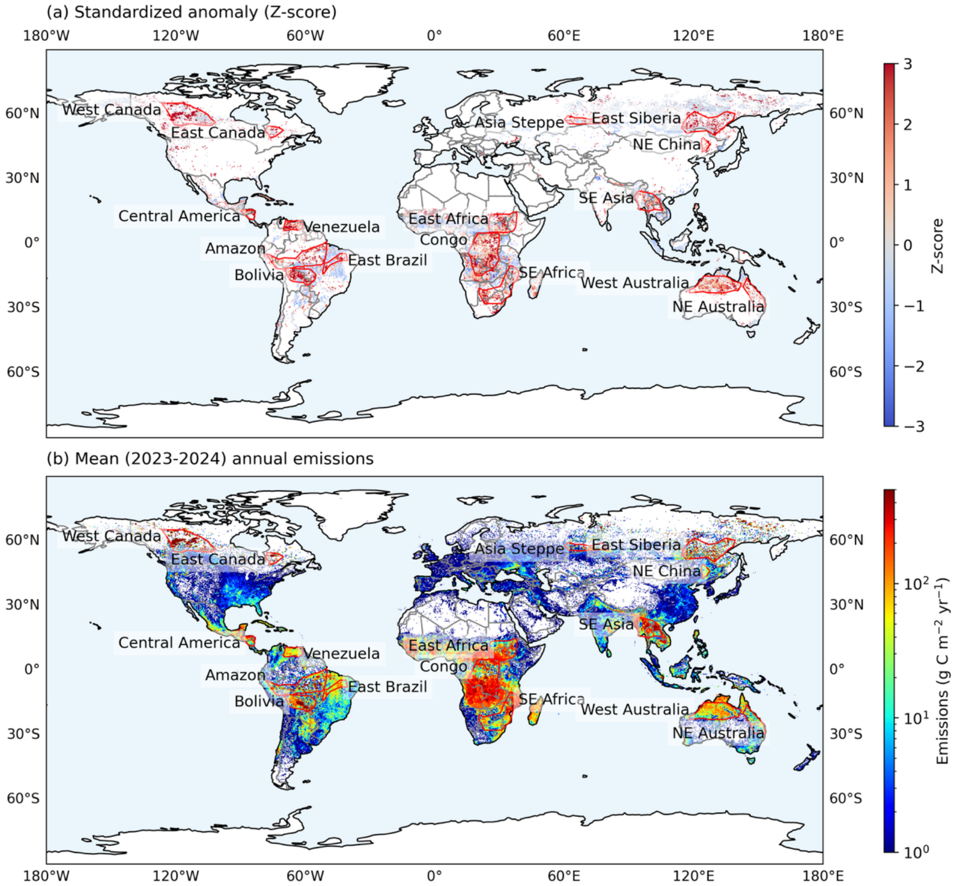

Figure 9. Global maps of (a) standardized anomalies and (b) annual mean fire emissions from GFED5NRT averaged over 2023–2024. Red polygons indicate identified regional fire events during 2023–2024.

Emissions from individual extreme regions ranged from 5 to 68 standard deviations above their respective climatological means. The highest relative anomalies, exceeding three times the climatological mean, occurred in eastern Canada, western Canada, and Bolivia. Several regions, including western Canada, Central America, and southeastern Siberia, experienced persistent extreme fire activity in both years (Fig. S6). Aggregated emission anomalies from these extreme regions reached 925 Tg C yr^{-1}, more than compensating for negative anomalies in other regions (-345 Tg C yr^{-1}), and resulting in a net positive global emissions anomaly of 463 Tg C yr^{-1}, equivalent to 2.15 standard deviations above the climatological mean.

3.5 Global wildfire situation updated by the GFED5NRT

The GFED5NRT dataset enables daily-scale quantification of burned area and fire-related emissions, substantially enhancing our ability to monitor evolving fire activity and its impacts. By providing timely estimates of burned area and emissions, GFED5NRT supports applications such as fire danger assessment, simulation and forecasting of smoke-driven air quality impacts, and rapid response to both direct fire hazards and downstream environmental and public health risks.

Figure 10 illustrates an example operational update, showing daily and cumulative global and regional fire through a selected date. Figures S7 and S8 further demonstrate the utility of the dataset by highlighting two extreme fire events—one in BONA (2023) and another in SHSA (2024)—and placing them in the context of historical variability captured by the GFED5NRT datasets.

GFED5NRT, updated on 2025-10-12

(a) Daily global and regional fire emissions (Tg C / day)

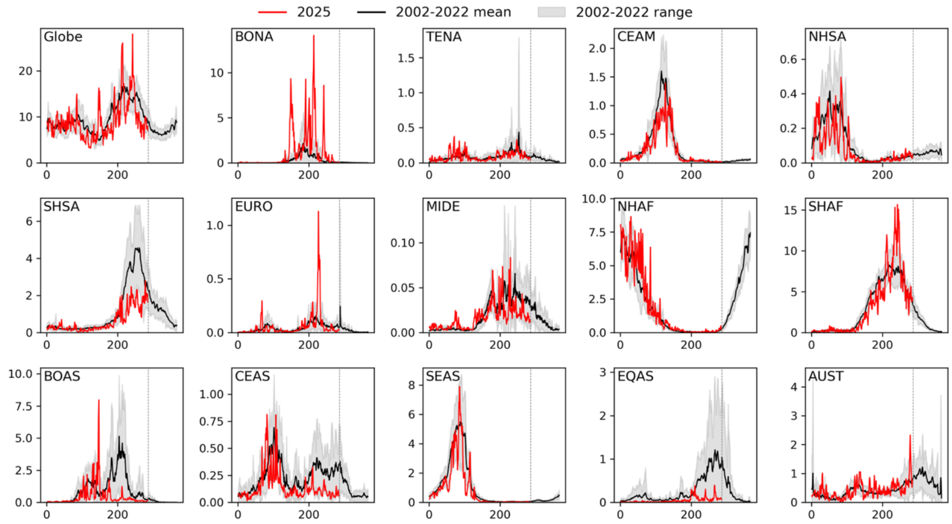

(b) Cumulative global and regional fire emissions (Tg C)

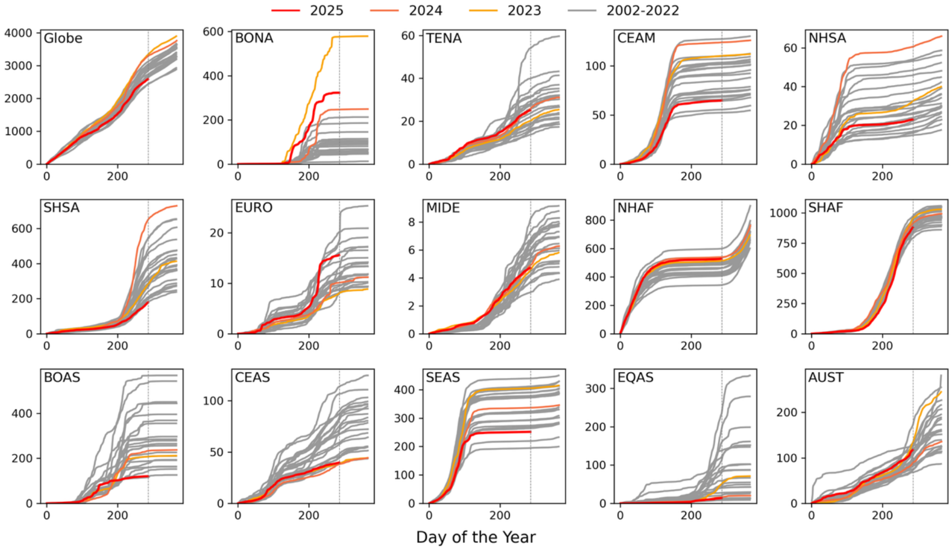

Figure 10. Example summary figures (updated on Oct 12, 2025) automatically generated by the GFED5NRT system. (a) Daily fire emission sums (Tg C day^{-1}) globally and by GFED regions. Red lines show GFED5NRT data for 2025. Black lines and gray areas indicate the historical mean and ±1 standard deviation based on 2002-

2022. (b) Cumulative fire emissions up to the reference date. Red, dark orange, orange, and gray lines represent 2025, 2024, 2023, and individual years from 2002-2022, respectively.

4. Data availability

The reprocessed 2023-2024 GFED5NRT datasets are publicly archived in the open-access Zenodo repository (https://zenodo.org/records/18702700; Chen et al., 2026). Routinely updated GFED5NRT products, including the reprocessed 2023–2024 data, are freely accessible at https://www.globalfiredata.org. The Python-based framework used to generate these products is openly available at https://github.com/ychenzgithub/GFED5NRT.

5. Conclusions

The accelerating orbital drift and imminent decommission of the Terra and Aqua satellites necessitate fusing fire records derived from these platforms with other higher-resolution, continuous data streams. The GFED5NRT dataset presented here represents a first step toward addressing this challenge by providing a temporally consistent, extended record of burned area and fire emissions derived from VIIRS active-fire observations. GFED5NRT advances the GFED framework by integrating VIIRS data through a two-step scaling approach that uses region- and biome-specific effective fire area and fuel consumption look-up tables. This design preserves continuity with the established GFED5 product while extending the record beyond 2022. By combining GFED5 and GFED5NRT, we construct a near-real-time fire dataset that enables a more robust assessment of recent fire variability at regional and global scales. The new fire observations from GFED5NRT reveal record-breaking carbon emissions from fires in 2023 in boreal North America and in 2024 in South America. Our analysis also confirms a significant global decline in burned area since 2002, driven primarily by reduced burning in Northern Hemisphere Africa and boreal and central Asia. However, this downward trend is likely weaker than previously reported by Andela et al. (2017) and Chen et al. (2023) due to higher levels of burning in Southern Hemisphere Africa, Australia, and boreal North America in the last two years. Global fire emissions remain relatively stable (van der Werf et al., 2025), with recent increases in North and South America balanced by declines in Asia.

Despite these advances, several limitations remain. In GFED5NRT, fuel consumption estimates and land-cover classifications are assumed to be static, which limits accuracy and interpretability in a rapidly evolving fire–climate–land-use system. In addition, errors in the empirical relationships between VIIRS active fire detections and GFED5 burned area contribute to substantially higher uncertainty in GFED5NRT compared with the original GFED5 time series. We estimate these additional uncertainties to be on the order of at least 12–45% for burned area, depending on region (Fig. S3), and therefore urge caution when using GFED5NRT to assess regional-scale trends in fire activity. The product is expected to be more robust when aggregated over large spatial scales and longer time periods, whereas analyses at smaller spatial scales (e.g., individual countries or subnational regions) may be associated with substantially higher uncertainties. Uncertainty is further compounded by the known limitations of using active fire observations as a proxy for burned area, which include obscuration by cloud cover and thick smoke, and more fundamentally the instantaneous nature of active fire detections versus the cumulative nature of burned area.

Currently, GFED5NRT is implemented at daily temporal resolution based on VIIRS active fire products. However, many fire-related applications, such as rapid response and smoke transport modeling, require sub-daily information and short-term forecasts. Previous studies have addressed this need by parameterizing diurnal fire cycles using fire radiative power observations from geostationary satellites (Andela et al., 2015; Xu et al., 2017), and the standard GFED5 framework incorporates climatological hourly cycles derived from GOES observations (van der Werf et al., 2025). More recent efforts have further advanced these approaches by fusing observations from multiple polar-orbiting and geostationary sensors (Li et al., 2022; Zhang et al., 2012; Zheng et al., 2021). Incorporating such multi-sensor strategies into future GFEDNRT developments would enable estimation of sub-daily fire variability, substantially enhancing the dataset's value for real-time air quality forecasting and fire behavior monitoring.

Another critical next step is the development of a global multi-decade fire reanalysis that harmonizes burned area time series from MODIS and VIIRS with higher-resolution observations from Sentinel-2 and Landsat. In parallel, harmonizing surface reflectance time series across MODIS, VIIRS, and Landsat would enable the development of a dynamic fuels model that explicitly accounts for evolving disturbance regimes, climate variability, and land-use change over decadal timescales. These needs underscore the importance of sustained investment in VIIRS science products within the United States. Incorporating complementary land cover datasets, such as those from the Tropical Moist Forest (Vancutsem et al., 2021) and MapBiomas (Souza et al., 2020; Alencar et al., 2022), also offers substantial potential to improve estimates of deforestation-related fire emissions. While such an approach would not replace GFED5NRT, which is designed for rapid assessment, it would likely yield a more temporally homogeneous dataset better suited for retrospective analyses of long-term trends (e.g., as the backbone for a future GFED6 assessment).

Acknowledgements

We gratefully acknowledge funding support from NASA's Earth Information System Fire Project, Fire Sense Technology Program (80NSSC24K1823), Fire Sense Implementation Team (80NSSC24K1317), Modelling, Analysis and Prediction Program (80NSSC21K1362), and Carbon Monitoring System Program (80NSSC25K7211). Additional support was provided by the US National Science Foundation (RISE-2425932), the US Dept. of Energy Office of Science RUBISCO Science Focus Area, and the CALIPSO (Carbon Loss In Plants, Soils and Oceans) project, funded through the generosity of Eric and Wendy Schmidt by recommendation of the Schmidt Science program.

Competing interests

The authors declare that they have no conflict of interest.

References

Ahmadov, R., Grell, G., James, E., Csiszar, I., Tsidulko, M., Pierce, B., McKeen, S., Benjamin, S., Alexander, C., Pereira, G., Freitas, S., & Goldberg, M. (2017). Using VIIRS fire radiative power data to simulate biomass burning emissions, plume rise and smoke transport in a real-time air quality modeling system. *Proceedings of the 2017 IEEE International Geoscience and Remote Sensing Symposium (IGARSS)*, 2806–2808. https://doi.org/10.1109/IGARSS.2017.8127581

Alencar, A. A. C., Arruda, V. L. S., Silva, W. V., Conciani, D. E., Costa, D. P., Crusco, N., Duverger, S. G., et al. (2022). Long-term Landsat-based monthly burned area dataset for the Brazilian biomes using deep learning. *Remote Sensing, 14*(11), 2510. https://doi.org/10.3390/rs14112510

Andela, N., Kaiser, J. W., van der Werf, G. R., & Wooster, M. J. (2015). New fire diurnal cycle characterizations to improve fire radiative energy assessments made from MODIS observations. *Atmospheric Chemistry and Physics, 15*(15), 8831–8846. https://doi.org/10.5194/acp-15-8831-2015

Andela, N., Morton, D. C., Giglio, L., Chen, Y., van der Werf, G. R., Kasibhatla, P. S., DeFries, R. S., Collatz, G. J., Hantson, S., Kloster, S., & Bachelet, D. (2017). A human-driven decline in global burned area. *Science, 356*(6345). https://doi.org/10.1126/science.aal4108

Balch, J. K., Abatzoglou, J. T., Joseph, M. B., Koontz, M. J., Mahood, A. L., McGlinchy, J., Cattau, M. E., & Williams, A. P. (2022). Warming weakens the night-time barrier to global fire. *Nature, 602*(7897), 442–448. https://doi.org/10.1038/s41586-021-04325-1

Binte Shahid, S., Lacey, F. G., Wiedinmyer, C., Yokelson, R. J., & Barsanti, K. C. (2024). NEIVAv1.0: Next-generation emissions inventory expansion of Akagi et al. (2011) version 1.0. *Geoscientific Model Development, 17*(21), 7679–7711. https://doi.org/10.5194/gmd-17-7679-2024

Chen, B., Wu, S., Jin, Y., Song, Y., Wu, C., Venevsky, S., Xu, B., Webster, C., & Gong, P. (2024). Wildfire risk for global wildland–urban interface areas. *Nature Sustainability*. https://doi.org/10.1038/s41893-024-01291-0

Chen, Y., Hall, J., van Wees, D., Andela, N., Hantson, S., Giglio, L., van der Werf, G. R., Morton, D. C., & Randerson, J. T. (2023). Multi-decadal trends and variability in burned area from the fifth version of the Global Fire Emissions Database (GFED5). *Earth System Science Data, 15*(11), 5227–5259. https://doi.org/10.5194/essd-15-5227-2023

Chen, Y., van der Werf, G., Mu, M., van Wees, D., Hall, J., Giglio, L., Vernooij, R., Morton, D., Xu, L., Liu, T., Scholten, R., Coffield, S., Follette-Cook, M., Ott, L., & Randerson, J. (2026). GFED5NRT: Global Fire Emissions Database Near-Real-Time Extension (V5.1) [Data set]. Zenodo. https://doi.org/10.5281/zenodo.18702700

Cunningham, C. X., Williamson, G. J., & Bowman, D. M. J. S. (2024). Increasing frequency and intensity of the most extreme wildfires on Earth. *Nature Ecology & Evolution, 8*(8), 1420–1425. https://doi.org/10.1038/s41559-024-02452-2

Darmenov, A., & da Silva, A. (2015). *The quick fire emissions dataset (QFED): Documentation of versions 2.1, 2.2 and 2.4* (NASA TM-2013-104606; NASA Technical Report Series on Global Modeling and Data Assimilation). NASA.

Friedl, M., & Sulla-Menashe, D. (2019). *MCD12Q1 MODIS/Terra+Aqua land cover type yearly L3 global 500m SIN grid V006*. NASA EOSDIS Land Processes DAAC. https://doi.org/10.5067/MODIS/MCD12Q1.006

Friedlingstein, P., O'Sullivan, M., Jones, M. W., Andrew, R. M., Hauck, J., Landschützer, P., … Zeng, J. (2025). Global carbon budget 2024. *Earth System Science Data, 17*, 965–1039. https://doi.org/10.5194/essd-17-965-2025

Giglio, L., Boschetti, L., Roy, D. P., Hall, J. V., Zubkova, M., Humber, M., Huang, H., & Oles, V. (2025). The NASA VIIRS burned area product, global validation, and intercomparison with the NASA MODIS burned area product. *Remote Sensing of Environment, 331*, 115006. https://doi.org/10.1016/j.rse.2025.115006

Giglio, L., Boschetti, L., Roy, D. P., Humber, M. L., & Justice, C. O. (2018). The Collection 6 MODIS burned area mapping algorithm and product. *Remote Sensing of Environment, 217*, 72–85. https://doi.org/10.1016/j.rse.2018.08.005

Giglio, L., Randerson, J. T., van der Werf, G. R., Kasibhatla, P. S., Collatz, G. J., Morton, D. C., & DeFries, R. S. (2010). Assessing variability and long-term trends in burned area by merging multiple satellite fire products. *Biogeosciences, 7*(3), 1171–1186. https://doi.org/10.5194/bg-7-1171-2010

Giglio, L., van der Werf, G. R., Randerson, J. T., Collatz, G. J., & Kasibhatla, P. (2006). Global estimation of burned area using MODIS active fire observations. *Atmospheric Chemistry and Physics, 6*, 957–974. https://doi.org/10.5194/acp-6-957-2006

Gumbricht, T., Roman-Cuesta, R. M., Verchot, L., Herold, M., Wittmann, F., Householder, E., Herold, N., & Murdiyarso, D. (2017). An expert system model for mapping tropical wetlands and peatlands reveals South America as the largest contributor. *Global Change Biology, 23*(9), 3581–3599. https://doi.org/10.1111/gcb.13689

Guo, Y., Wang, J., Ge, Y., & Zhou, C. (2024). Global expansion of wildland–urban interface intensifies human exposure to wildfire risk in the 21st century. *Science Advances, 10*(45), eado9587. https://doi.org/10.1126/sciadv.ado9587

Hall, J. V., Argueta, F., Zubkova, M., Chen, Y., Randerson, J. T., & Giglio, L. (2024). GloCAB: Global cropland burned area from mid-2002 to 2020. *Earth System Science Data, 16*(2), 867–885.

Hall, J. V., Loboda, T. V., Giglio, L., & McCarty, G. W. (2016). A MODIS-based burned area assessment for Russian croplands: Mapping requirements and challenges. *Remote Sensing of Environment, 184*, 506–521. https://doi.org/10.1016/j.rse.2016.07.022

Jain, P., Castellanos-Acuna, D., Coogan, S. C. P., Abatzoglou, J. T., & Flannigan, M. D. (2022). Observed increases in extreme fire weather driven by atmospheric humidity and temperature. *Nature Climate Change, 12*(1), 63–70.

Jones, M. W., Abatzoglou, J. T., Veraverbeke, S., Andela, N., Lasslop, G., Forkel, M., Smith, A. J. P., Burton, C., Betts, R. A., van der Werf, G. R., Sitch, S., Canadell, J. G., Santín, C., Kolden, C., Doerr, S. H., & Le Quéré, C. (2022). Global and regional trends and drivers of fire under climate change. *Reviews of Geophysics*.

Jones, M. W., Kelley, D. I., Burton, C. A., Di Giuseppe, F., Barbosa, M. L. F., Brambleby, E., Hartley, A. J., Lombardi, A., Mataveli, G., McNorton, J. R., Spuler, F. R., Wessel, J. B., Abatzoglou, J. T., Anderson, L. O., Andela, N., Archibald, S., Armenteras, D., Burke, E., Carmenta, R., … Xanthopoulos, G. (2024). State of wildfires 2023–2024. *Earth System Science Data, 16*(8), 3601–3685. https://doi.org/10.5194/essd-16-3601-2024

Justice, C. O., Giglio, L., Korontzi, S., Owens, J., Morisette, J. T., Roy, D., Descloitres, J., Alleaume, S., Petitcolin, F., & Kaufman, Y. (2002). The MODIS fire products. *Remote Sensing of Environment, 83*(1–2), 244–262. https://doi.org/10.1016/S0034-4257(02)00076-7

Kaiser, J. W., Heil, A., Andreae, M. O., Benedetti, A., Chubarova, N., Jones, L., Morcrette, J.-J., Razinger, M., Schultz, M. G., Suttie, M., & van der Werf, G. R. (2012). Biomass burning emissions estimated with a global fire assimilation system based on observed fire radiative power. *Biogeosciences, 9*(1), 527–554. https://doi.org/10.5194/bg-9-527-2012

Libonati, R., DaCamara, C., Setzer, A., Morelli, F., & Melchiori, A. (2015). An algorithm for burned area detection in the Brazilian Cerrado using 4 μm MODIS imagery. *Remote Sensing, 7*(12), 15782–15803. https://doi.org/10.3390/rs71215782

Li, F., Zhang, X., Kondragunta, S., Lu, X., Csiszar, I., & Schmidt, C. C. (2022). Hourly biomass burning emissions product from blended geostationary and polar-orbiting satellites for air quality forecasting applications. *Remote Sensing of Environment, 281*, 113237. https://doi.org/10.1016/j.rse.2022.113237

Loeb, N. G., Doelling, D. R., Kato, S., Su, W., Mlynczak, P. E., & Wilkins, J. C. (2024). Continuity in top-of-atmosphere Earth radiation budget observations. *Journal of Climate, 37*(23), 6093–6108. https://doi.org/10.1175/JCLI-D-24-0180.1

Mu, M., Randerson, J. T., Van Der Werf, G. R., Giglio, L., Kasibhatla, P., Morton, D., ... & Wennberg, P. O. (2011). Daily and 3-hourly variability in global fire emissions and consequences for atmospheric model predictions of carbon monoxide. *Journal of Geophysical Research: Atmospheres*, *116*(D24).

Parkinson, C. L. (2022). The Earth-observing Aqua satellite mission: 20 years and counting. *Earth and Space Science, 9*(9), e2022EA002481. https://doi.org/10.1029/2022EA002481

Pelletier, F., Cardille, J. A., Wulder, M. A., White, J. C., & Hermosilla, T. (2024). Revisiting the 2023 wildfire season in Canada. *Science of Remote Sensing*, 10, 100145. https://doi.org/10.1016/j.srs.2024.100145

Potter, C. S., Randerson, J. T., Field, C. B., Matson, P. A., Vitousek, P. M., Mooney, H. A., & Klooster, S. A. (1993). Terrestrial ecosystem production: A process model based on global satellite and surface data. *Global Biogeochemical Cycles, 7*(4), 811–841. https://doi.org/10.1029/93GB02725

Randerson, J. T., Chen, Y., van der Werf, G. R., Rogers, B. M., & Morton, D. C. (2012). Global burned area and biomass burning emissions from small fires. *Journal of Geophysical Research: Biogeosciences, 117*, G04012. https://doi.org/10.1029/2012JG002128

Román, M. O., Justice, C., Paynter, I., Boucher, P. B., Devadiga, S., Endsley, A., Erb, A., Friedl, M., Gao, H., Giglio, L., Gray, J. M., Hall, D., Hulley, G., Kimball, J., Knyazikhin, Y., Lyapustin, A., Myneni, R. B., Noojipady, P., Pu, J., … Wolfe, R. (2024). Continuity between NASA MODIS Collection 6.1 and VIIRS Collection 2 land products. *Remote Sensing of Environment, 302*, 113963. https://doi.org/10.1016/j.rse.2023.113963

Schroeder, W., Giglio, L., & Hall, J. (2024). *Collection 2 Visible Infrared Imaging Radiometer Suite (VIIRS) 375-m active fire product user's guide* (Version 1.2).

Schroeder, W., Ruminski, M., Csiszar, I., Giglio, L., Prins, E., Schmidt, C., & Morisette, J. (2008). Validation analyses of an operational fire monitoring product: The Hazard Mapping System. *International Journal of Remote Sensing, 29*(20), 6059–6066. https://doi.org/10.1080/01431160802235845

Schug, F., Bar-Massada, A., Carlson, A. R., Cox, H., Hawbaker, T. J., Helmers, D., Hostert, P., Kaim, D., Kasraee, N. K., Martinuzzi, S., Mockrin, M. H., Pfoch, K. A., & Radeloff, V. C. (2023). The global wildland–urban interface. *Nature, 621*(7977), 94–99. https://doi.org/10.1038/s41586-023-06320-0

Seiler, W., & Crutzen, P. J. (1980). Estimates of gross and net fluxes of carbon between the biosphere and the atmosphere from biomass burning. *Climatic Change, 2*(3), 207–247. https://doi.org/10.1007/BF00137988

Souza, C. M., Shimbo, J. Z., Rosa, M. R., Parente, L. L., Alencar, A. A., Rudorff, B. F. T., Hasenack, H., Matsumoto, M., Ferreira, L. G., Souza-Filho, P. W. M., de Oliveira, S. W., Rocha, W. F., Fonseca, A. V., Marques, C. B., Diniz, C. G., Costa, D., Monteiro, D., Rosa, E. R., Vélez-Martin, E., … Azevedo, T. (2020). Reconstructing three decades of land use and land cover changes in Brazilian biomes with Landsat archive and Earth Engine. *Remote Sensing, 12*(17), 2735. https://doi.org/10.3390/rs12172735

Tang, W., He, C., Emmons, L., & Zhang, J. (2024). Global expansion of wildland–urban interface (WUI) and WUI fires: Insights from a multiyear worldwide unified database (WUWUI). *Environmental Research Letters, 19*.

Teymoor Seydi, S., Abatzoglou, J. T., Jones, M. W., Kolden, C. A., Filippelli, G., Hurteau, M. D., AghaKouchak, A., Luce, C. H., Miao, C., & Sadegh, M. (2025). Increasing global human exposure to wildland fires despite declining burned area. *Science, 389*(6762), 826–829. https://doi.org/10.1126/science.adu6408

van der Werf, G. R., Randerson, J. T., Giglio, L., Collatz, G. J., Kasibhatla, P. S., & Arellano, A. F. (2006). Interannual variability in global biomass burning emissions from 1997 to 2004. *Atmospheric Chemistry and Physics, 6*(11), 3423–3441. https://doi.org/10.5194/acp-6-3423-2006

van der Werf, G. R., Randerson, J. T., Giglio, L., Collatz, G. J., Mu, M., Kasibhatla, P. S., Morton, D. C., DeFries, R. S., Jin, Y., & van Leeuwen, T. T. (2010). Global fire emissions and the contribution of deforestation, savanna, forest, agricultural, and peat fires (1997–2009). *Atmospheric Chemistry and Physics, 10*(23), 11707–11735. https://doi.org/10.5194/acp-10-11707-2010

van der Werf, G. R., Randerson, J. T., Giglio, L., van Leeuwen, T. T., Chen, Y., Rogers, B. M., Mu, M., van Marle, M. J. E., Morton, D. C., Collatz, G. J., Yokelson, R. J., & Kasibhatla, P. S. (2017). Global fire emissions estimates during 1997–2016. *Earth System Science Data, 9*(2), 697–720. https://doi.org/10.5194/essd-9-697-2017 van der Werf, G. R., Randerson, J. T., van Wees, D., Chen, Y., Giglio, L., Hall, J., Roland, V., Mu, M., Binte Shahid, S., Barsanti, K. C., Yokelson, R., & Morton, D. C. (2025). Landscape fire emissions from the 5th version of the Global Fire Emissions Database (GFED5). *Scientific Data, 12*(1), 1870. https://doi.org/10.1038/s41597-025-06127-w

van Wees, D., van der Werf, G. R., Randerson, J. T., Rogers, B. M., Chen, Y., Veraverbeke, S., Giglio, L., & Morton, D. C. (2022). Global biomass burning fuel consumption and emissions at 500-m spatial resolution based on the Global Fire Emissions Database (GFED). *Geoscientific Model Development*. https://doi.org/10.5194/gmd-2022-132

Vancutsem, C., Achard, F., Pekel, J. F., Vieilledent, G., Carboni, S., Simonetti, D., Gallego, J., Aragão, L. E. O. C., & Nasi, R. (2021). Long-term (1990–2019) monitoring of forest cover changes in the humid tropics. *Science Advances, 7*(10). https://doi.org/10.1126/sciadv.abe1603

Wiedinmyer, C., Akagi, S. K., Yokelson, R. J., Emmons, L. K., Al-Saadi, J. A., Orlando, J. J., & Soja, A. J. (2011). The Fire INventory from NCAR (FINN): A high-resolution global model to estimate emissions from open burning. *Geoscientific Model Development, 4*(3), 625–641. https://doi.org/10.5194/gmd-4-625-2011

Wiedinmyer, C., Kimura, Y., McDonald-Buller, E. C., Emmons, L. K., Buchholz, R. R., Tang, W., Seto, K., Joseph, M. B., Barsanti, K. C., Carlton, A. G., & Yokelson, R. (2023). The Fire Inventory from NCAR version 2.5: An updated global fire emissions model for climate and chemistry applications. *Geoscientific Model Development, 16*(13), 3873–3891. https://doi.org/10.5194/gmd-16-3873-2023

Xu, W., Wooster, M. J., Kaneko, T., He, J., Zhang, T., & Fisher, D. (2017). Major advances in geostationary fire radiative power (FRP) retrieval over Asia and Australia stemming from use of Himawari-8 AHI. *Remote Sensing of Environment, 193*, 138–149. https://doi.org/10.1016/j.rse.2017.02.024

Zhang, X. Y., Kondragunta, S., Ram, J., Schmidt, C., & Huang, H. C. (2012). Near-real-time global biomass burning emissions product from geostationary satellite constellation. *Journal of Geophysical Research: Atmospheres, 117*. https://doi.org/10.1029/2011JD016802

Zhao, J., Zheng, B., Ciais, P., Chen, Y., Gasser, T., Canadell, J. G., ... & Zhang, Q. (2025). Global warming amplifies wildfire health burden and reshapes inequality. *Nature*, 647(8091), 928-934. https://doi.org/10.1038/s41586-025-09612-9

Zheng, Y., Liu, J., Jian, H., Fan, X., & Yan, F. (2021). Fire diurnal cycle derived from a combination of the Himawari-8 and VIIRS satellites to improve fire emission assessments in southeast Australia. *Remote Sensing, 13*(15), 2852. https://doi.org/10.3390/rs13152852